Extended Wannier-Stark ladder and electron-pair Bloch oscillations in dimerized non-Hermitian systems

H. P. Zhang and Z. Song*
School of Physics, Nankai University, Tianjin 300071, China

(Received 2 April 2024; revised 5 July 2024; accepted 31 July 2024; published 12 August 2024)

In the Hermitian regime, the Wannier-Stark ladder characterizes the eigenstates of an electron in a periodic potential with an applied static electric field. In this work, we extend this concept to the complex regime for a periodic non-Hermitian system under a linear potential. We show that although the energy levels can be complex, they are still equally spaced by a real Bloch frequency. This ensures single-particle Bloch oscillations with a damping (or growing) rate. The system can also support standard two-particle Bloch oscillations under certain conditions. We propose two types of dimerized non-Hermitian systems to demonstrate our results. In addition, we also propose a scheme to demonstrate the results of particle-pair dynamics in a single-particle two-dimensional $\mathcal{PT}$-symmetric square lattice.

DOI: 10.1103/PhysRevB.110.064310

I. INTRODUCTION

Bloch oscillation is a feature of the dynamics of an electron under a periodic potential and an external electric field [1]. Within the Hermitian regime, Bloch oscillations occur due to the acceleration of an electron by an electric field, which is described by the acceleration theorem in reciprocal space [2], and subsequent Bragg reflections from the periodic lattice potential at the boundaries of the first Brillouin zone. An alternative description can be given in the framework of traditional quantum mechanics. In 1960, Wannier [3] theoretically proved that the eigenstates of an electron in a periodic potential with an applied static electric field can be described by the Wannier-Stark ladder. Then, the periodic dynamics arise from the Wannier-Stark ladder, which consists of quantized equidistant energy levels separated by the Bloch frequency [4]. As a universal wave phenomenon, it has attracted much attention from various research areas due to experimental observations. It has been reported that such periodic dynamics are observed in a semiconductor superlattice [5], ultracold atoms in the optical lattice [6–9], and many other systems sequentially [10–14].

Theoretically, the investigation of the Wannier-Stark ladder has been extended to new frontiers, such as non-Hermitian systems [15,16]. Recent works [17–19] show that a non-Hermitian hopping term, including asymmetrical and complex strengths, remains the reality of the Wannier-Stark ladder. A non-Hermitian system can exhibit exclusive dynamics that never occur in a Hermitian system, especially when complex energy is involved. Importantly, non-Hermitian dynamics can be observed in experiments. In contrast to non-Hermitian optical systems, a few-body non-Hermitian Hamiltonian can be implemented through a scheme that is analogous to heralded entanglement protocols [20]. This raises the question of whether an extended Wannier-Stark ladder, which consists of quantized equidistant *complex* energy levels, but separated by the *real* Bloch frequency, can emerge in a periodic non-Hermitian system under a linear potential.

In this work, we focus on the effects of a linear potential on periodic systems, using the tight-binding model as a framework for analysis. This model is widely used in condensed-matter physics to describe the behavior of electrons in crystalline structures. We extend the concept of the Wannier-Stark ladder, which is traditionally used to describe eigenstates in a periodic potential with an electric field in Hermitian systems, to non-Hermitian systems with complex eigenvalues. This extension is significant because it broadens the analytical tools available for studying the dynamics of such systems. Such an extension of the Wannier-Stark ladder to the complex regime enables the analytical prediction of the dynamics of many non-Hermitian systems with a fixed number of particles. This provides the prediction of Bloch oscillations in non-Hermitian systems without the need for complex numerical simulations. To demonstrate this point, two types of dimerized non-Hermitian systems are proposed as examples to illustrate the research findings. This indicates that dimerized non-Hermitian systems can support both single-particle and two-particle Bloch oscillations. These oscillations are characterized by a damping (or growing) rate, which reflects the temporal evolution of the quantum state. Furthermore, we show that the extended Wannier-Stark ladder concept, initially developed for one-dimensional (1D) systems, can also be applied to 2D systems. This broadens the applicability of the concept and opens up new avenues for related research. We propose a scheme involving electron-, boson-, and spinless fermion-pair dynamics in a single-particle 2D $\mathcal{PT}$-symmetric square lattice to demonstrate the results. Here, $\mathcal{PT}$ symmetry [21–28], a combination of parity and time-reversal symmetry, is a key concept in non-Hermitian physics [29] and can lead to real eigenvalues under certain conditions, especially for discrete

*Contact author: songtc@nankai.edu.cn

systems [30,31]. Our findings pave the way for further investigations into a wide variety of periodic systems under the influence of a linear potential. This could have significant implications for understanding and designing devices with tailored properties. In addition, this work contributes to the understanding of non-Hermitian systems and provides new tools for their analysis.

This paper is organized as follows. In Sec. II, we present a general formalism for Hamiltonians with ramped translational symmetry and show the existence of energy ladders, referred to as extended Wannier-Stark ladders, regardless of the Hermiticity of the systems. In Sec. III, we propose two types of non-Hermitian dimer systems to demonstrate the extended Wannier-Stark ladders. In Sec. IV, we study single-particle damping Bloch oscillations. Section V is devoted to the 2D representation of two-electron, two-boson, and two-spinless fermion dynamics in a 1D system. Finally, we summarize our results in Sec. VI.

II. GENERAL FORMALISM

In this section, we present a general formalism supporting the extended Wannier-Stark ladder. First, we propose a class of Hamiltonians, including non-Hermitian ones, which possesses a ramped translational symmetry. Second, we show that such Hamiltonians can have several sets of energy ladders: the energy levels can be complex, but the level spacing can be real valued and identical. The translational operators across two neighboring unit cells act as ladder operators, generating a set of eigenstates from an obtained eigenstate.

A. Model and symmetry

We start with a general tight-binding model with the Hamiltonians in the following forms:

$$H = H_0 + \omega \sum_{j=-\infty}^{\infty} j a_j^\dagger a_j, \tag{1}$$

$$H_0 = \sum_{i,j=-\infty}^{\infty} J_{ij} a_i^\dagger a_j, \tag{2}$$

where $a_i^\dagger$ (a_i) is the boson or fermion creation (annihilation) operator at the ith site. It is an infinite chain lattice with a unit cell consisting of n_0 different types of sites. This means that the Hamiltonian H_0 obeys the translational symmetry

$$T_{n_0} H_0 T_{n_0}^{-1} = H_0, \tag{3}$$

where T_{n_0} is the translational operator defined as

$$T_{n_0} a_j^\dagger T_{n_0}^{-1} = a_{j+n_0}^\dagger, \quad T_{n_0} a_j T_{n_0}^{-1} = a_{j+n_0}. \tag{4}$$

In addition, there are no other restrictions on the set of coefficients $\{J_{ij}\}$. Figure 1 is a schematic of the system. In this sense, the following conclusion still holds for the non-Hermitian Hamiltonian H_0. The non-Hermiticity arises from the case with $J_{ij} \neq (J_{ji})^*$, which corresponds to non-Hermitian hopping strength for $i \neq j$ and complex on-site potentials for $i = j$. In previous work [32], a simple case with $J_{j(j+1)} = J_{(j+1)j} = J$ ($n_0 = 1$) is considered for complex J. The exact solution indicates that the energy levels are always real and equidistant, in accordance with the above conclusion.

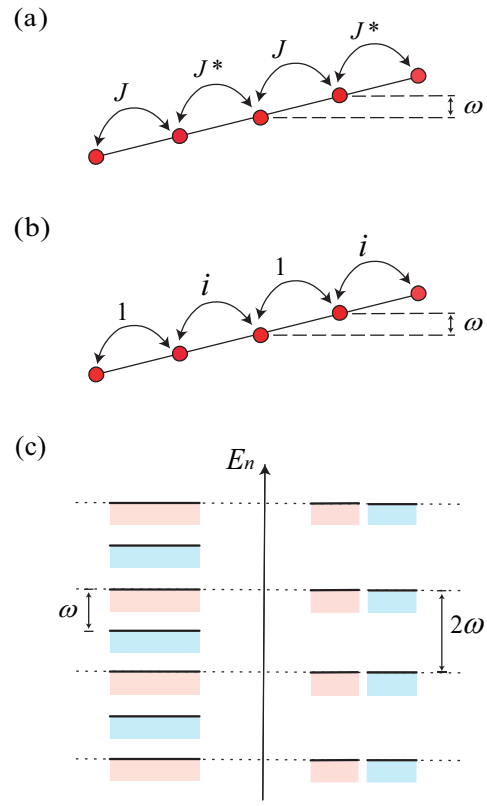

FIG. 1. Schematic illustrations of (a) the Hamiltonian in Eq. (11) and (b) the Hamiltonian in Eq. (16), which correspond to the adjacent hopping strengths J, J^* and 1, i, respectively. The on-site potential is tilted with slope ω. It is shown that the latter has $\mathcal{PT}$ symmetry, being a pseudo-Hermitian system. (c) Energy level structure diagrams for the Hamiltonians of panels (a) and (b). The solid line represents the real part of the energy level with isoenergetic distance ω for panel (a) and 2ω for panel (b). The red and blue blocks represent the positive imaginary part and the negative imaginary part of the energy level, respectively. It can be seen that the energy spectrum on the right side is composed of conjugate energy levels, which correspond exactly to the $\mathcal{PT}$ symmetry of panel (b).

In general, the Hamiltonian H_0 can be block diagonalized due to translational symmetry, while it is difficult to diagonalize the Hamiltonian H with $n_0 > 1$, since term $\omega \sum_{j=-\infty}^{\infty} j a_j^\dagger a_j$ breaks the translational symmetry.

B. Ladder operators

However, the special structure of the linear potential ensures that H obeys

$$T_{n_0} H T_{n_0}^{-1} = H - n_0 \omega, \tag{5}$$

which is referred to as a ramped translational symmetry. Although this symmetry has no help in determining the explicit form of eigenstates, it reflects the relationships between the eigenstates.

Suppose we have a solution $|\psi_0\rangle$ of the Schrödinger equation corresponding to energy E_0,

$$H|\psi_0\rangle = E_0|\psi_0\rangle, \tag{6}$$

we always have

$$H(T_{n_0}|\psi_0\rangle) = (E_0 + n_0\,\omega)(T_{n_0}|\psi_0\rangle) \tag{7}$$

and

$$H\big(T_{n_0}^{-1}|\psi_0\rangle\big) = (E_0 - n_0\,\omega)\big(T_{n_0}^{-1}|\psi_0\rangle\big), \tag{8}$$

i.e., $T_{n_0}|\psi_0\rangle(T_{n_0}^{-1}|\psi_0\rangle)$ is also the eigenstate of H with eigenenergy $E_0+\omega$ ($E_0-\omega$). Operator T_{n_0} moves up the energy ladder by a step of $n_0\omega$ and the operator $T_{n_0}^{-1}$ moves down the energy ladder by a step of $n_0\omega$. We can then construct a set of eigenstates,

$$|\psi_n\rangle = \big(T_{n_0}\big)^n|\psi_0\rangle, \tag{9}$$

$n = 0, \pm1, \pm2, \ldots$, with eigenenergy

$$E_n = E_0 + nn_0\omega \tag{10}$$

Thus, we can conclude that the spectrum of H has equally spaced energy levels. The translational operator T_{n_0} acts as a ladder operator. This proof is independent of $\{J_{ij}\}$; i.e., it can be a complex number. We note that based on another eigenstate, $|\phi_0\rangle$, another set of eigenstates can be generated accordingly.

Applying the conclusion to the case with $J_{j(j+1)} = J_{(j+1)j} = J$ ($n_0 = 1$), the same result as that in Refs. [32,33] can be obtained for complex constant J. In the following, we focus on two types of non-Hermitian systems to demonstrate the application of our conclusion and reveal the pair dynamics.

III. DIMERIZED NON-HERMITIAN CHAINS

In the following, we focus on non-Hermitian systems for two cases with $n_0 = 2$. Figure 1 is a schematic for the structure and energy levels of two systems.

(i) $J_{2j(2j+1)} = J_{(2j+1)2j} = J$ and $J_{2j(2j-1)} = J_{(2j-1)2j} = J^*$. In this case, the Hamiltonian reads

$$H_0 = \sum_{l=-\infty}^{\infty}[J(a_{2l}^\dagger a_{2l+1} + \text{H.c.}) + J^*(a_{2l-1}^\dagger a_{2l} + \text{H.c.})]. \tag{11}$$

Figure 1(a) is a schematics of the system. A straightforward derivation shows that

$$\begin{aligned} T_2 H T_2^{-1} &= H - 2\omega, \\ T_1 H T_1^{-1} &= H^* - \omega. \end{aligned} \tag{12}$$

Starting from an arbitrary eigenstate $|\psi_0\rangle$ of H, a set of eigenstates can be generated as

$$|\psi_n\rangle = \begin{cases} (T_2)^l|\psi_0\rangle, & n = 2l, \\ \mathcal{T}(T_1)^{2l+1}|\psi_0\rangle, & n = 2l+1, \end{cases} \tag{13}$$

$l = 0, \pm1, \pm2, \ldots$, with eigenenergy

$$E_n = \begin{cases} E_0 + n\omega, & n = 2l, \\ E_0^* + n\omega, & n = 2l+1, \end{cases} \tag{14}$$

or in the compact form

$$|\psi_n\rangle = (\mathcal{T}T_1)^n|\psi_0\rangle,$$

with

$$E_n = (\mathcal{T})^n E_0 (\mathcal{T}^{-1})^n + n\omega \tag{15}$$

($n = 0, \pm1, \pm2, \ldots$), where $\mathcal{T}$ is the time-reversal operator defined as $\mathcal{T}\sqrt{-1}\mathcal{T}^{-1} = -\sqrt{-1}$. We can see that operator $\mathcal{T}T_1$ acts as a ladder operator. Considering the eigenstates in a single-particle invariant subspace, complete eigenstates can be constructed from an arbitrary eigenstate. The corresponding energy levels are complex: the real part has equal spacing, while the imaginary part is alternatively conjugated.

(ii) $J_{2j(2j+1)} = J_{(2j+1)2j} = 1$ and $J_{2j(2j-1)} = J_{(2j-1)2j} = i$. In this case, the Hamiltonian reads

$$H_0 = \sum_{l=-\infty}^{\infty}[(a_{2l}^\dagger a_{2l+1} + \text{H.c.}) + i(a_{2l-1}^\dagger a_{2l} + \text{H.c.})]. \tag{16}$$

Figure 1(b) is a schematics of the system. A straightforward derivation shows that

$$\begin{aligned} T_2 H T_2^{-1} &= H - 2\omega, \\ gHg^{-1} &= H^*, \end{aligned} \tag{17}$$

where the local gauge transformation is defined as

$$\begin{aligned} ga_{2l}g^{-1} &= (-1)^l a_{2l}, \\ ga_{2l+1}g^{-1} &= (-1)^l a_{2l+1}. \end{aligned} \tag{18}$$

Starting from an arbitrary eigenstate $|\psi_0\rangle$ of H, a set of eigenstates can be generated as

$$\begin{aligned} |\psi_l^+\rangle &= (T_2)^l|\psi_0\rangle, \\ |\psi_l^-\rangle &= \mathcal{T}g(T_2)^l|\psi_0\rangle \end{aligned} \tag{19}$$

($l = 0, \pm1, \pm2, \ldots$), with eigenenergy

$$\begin{aligned} E_l^+ &= E_0 + 2l\omega, \\ E_l^- &= E_0^* + 2l\omega. \end{aligned} \tag{20}$$

Here, without loss of generality, we assume that $\text{Im}E_0 > 0$. Considering the eigenstates in a single-particle invariant subspace, complete eigenstates can be constructed from an arbitrary eigenstate. The spectrum indicates that the Hamiltonian is pseudo-Hermitian, in which complex energy levels appear in the conjugate pair. This feature allows one to construct a two-particle subspace with all real energy levels. Considering a set of two-particle eigenstates $|\psi_l^+\rangle|\psi_l^-\rangle$, including electron, boson and spinless fermion, the corrsponding energy levels are $2\text{Re}(E_0) + 4l\omega$, forming a standard Wannier-Stark ladder. Additionally, as a starting point, E_0 and $|\psi_0\rangle$ can be obtained numerically for an infinite system by using the powerful Floquet operator method [34,35]. In Fig. 2, the plots of E_0 as a function of ω and the profiles of two typical $|\psi_0\rangle$ states are presented. We find that the real part of E_0 is a linear function of ω and the width of $|\psi_0\rangle$ strongly depends on the value of ω.

IV. BLOCH OSCILLATIONS

In this section, we investigate the dynamic feature of a system with an extended Wannier-Stark ladder. We will consider the single- and double-particle dynamics driven by the Hamiltonian in Eq. (16) with linear potential.

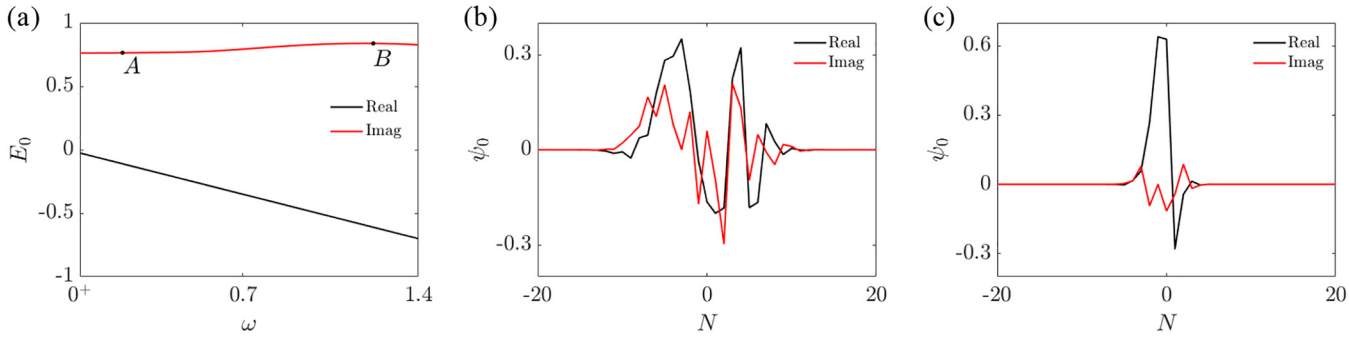

FIG. 2. Plots of E_0 and ψ_0 defined in Eqs. (20) and (19), respectively, for the Hamiltonian system (16) in a potential with slope ω. Panel (a) is the dependence curve of E_0 on ω. Panels (b) and (c) are the eigenfunctions for the systems at points A and B, where A and B correspond to $\omega = 0.2$ and 1.2, respectively. It can be observed that, when ω is small, the corresponding eigenfunction is wider, which corresponds to the pronounced Bloch oscillations that follow. When ω is larger, the eigenfunction noticeably narrows, which is not conducive to observing Bloch oscillations. The real part of E_0 is a linear function of ω.

Assuming that $|\psi_0\rangle$ is a single-particle eigenstate $|\psi_0\rangle$ of H with eigenenergy E_0, $|\psi_0\rangle$ can be expressed in the form

$$|\psi_0\rangle = \sum_{j=-\infty}^{\infty} f_j a_j^\dagger |0\rangle. \tag{21}$$

Then other eigenstates can be expressed in the forms

$$|\psi_l^+\rangle = \sum_{j=-\infty}^{\infty} f_{j-2l} a_j^\dagger |0\rangle,$$
$$|\psi_l^-\rangle = \sum_{j=-\infty}^{\infty} (-1)^{\mathrm{INT}(j/2)} f_{j-2l}^* a_j^\dagger |0\rangle, \tag{22}$$

with the eigenenergy $E_l^\pm$ in Eq. (20). For an arbitrary single-particle initial state

$$|\phi(0)\rangle = \sum_l (\alpha_l |\psi_l^+\rangle + \beta_l |\psi_l^-\rangle), \tag{23}$$

the time evolution of the state at time t is $|\phi(t)\rangle = e^{-iHt}|\phi(0)\rangle$. After a sufficiently long time, we have

$$|\phi(t)\rangle = e^{-iE_0 t} \sum_l \alpha_l e^{-i2l\omega t} |\psi_l^+\rangle, \tag{24}$$

which indicates that such a natural time evolution takes the role of projection to rule out the component of $|\psi_l^-\rangle$. Obviously, the state $e^{iE_0 t}|\phi(t)\rangle = \sum_l \alpha_l e^{-i2l\omega t}|\psi_l^+\rangle$ is a periodic with period π/ω. We can conclude that an initial state in the form $\sum_l \beta_l |\psi_l^-\rangle$ exhibits damping Bloch oscillation, while state $\sum_l \alpha_l |\psi_l^+\rangle$ suffices for growing Bloch oscillation. Notably, on the other hand, when we consider a two-particle initial state in the form $\sum_{l,l'} \gamma_{ll'} |\psi_l^+\rangle |\psi_{l'}^-\rangle$, a standard Bloch oscillation occurs. A simple example of such states is $|\phi(t)\rangle|\phi(t)\rangle^*$ for large t. We investigate the two-particle dynamics in an alternative way in the next section. To verify and demonstrate the above analysis, numerical simulations are performed to investigate the dynamic behavior driven by the non-Hermitian Hamiltonian with a complex Wannier-Stark ladder. We compute the temporal evolution for two types of initial states: (i) a Gaussian wave-packet state in the form

$$|\phi(0)\rangle = \sum_j e^{-\alpha^2 (j-j_0)^2} a_j^\dagger |0\rangle \tag{25}$$

($\alpha = 0.3$); and (ii) a site state at the j_0th site in the form $|\phi(0)\rangle = a_{j_0}^\dagger |0\rangle$. To present a complete profile of the evolved state, we take a mapping $|\phi(t)\rangle \to e^{-\lambda t}|\phi(t)\rangle$ by a prefactor to reduce the damping (or growing) rate. Obviously, the dynamics exhibit a normal Bloch oscillation when taking $\lambda = \mathrm{Im}E_0$. For a given initial state, the Dirac probability distribution in real space for the evolved state $|\phi(t)\rangle$ is

$$P_n(t) = |\langle n|e^{-\lambda t}|\phi(t)\rangle|^2. \tag{26}$$

We plot $P_n(t)$ in Fig. 3 for several typical parameter values. These numerical results agree with our above analysis: (i) when taking $\lambda > \mathrm{Im}E_0$, the dynamics are damping periodic; and (ii) when taking $\lambda = \mathrm{Im}E_0$, the dynamics are periodic.

V. TWO-DIMENSIONAL SIMULATOR FOR ELECTRON-PAIR DYNAMICS

As shown above, the non-Hermitian dimerized Hamiltonians always have complex single-particle energy levels. The corresponding dynamics are no longer periodic. However, some many-particle energy levels can be real and equally spaced. In this section, we investigate the Bloch oscillations for a two-particle system and propose a 2D simulator to observe such dynamics in experiments. We consider electron, spinless fermion, and boson systems, respectively.

(i) For the electron system, the Hamiltonian reads

$$H_e = \sum_{j,\sigma=\uparrow,\downarrow} (c_{2j,\sigma}^\dagger c_{2j+1,\sigma} + \mathrm{H.c.}) + i \sum_{j,\sigma=\uparrow,\downarrow} (c_{2j-1,\sigma}^\dagger c_{2j,\sigma} + \mathrm{H.c.}) + \omega \sum_{j,\sigma=\uparrow,\downarrow} j n_{j,\sigma}, \tag{27}$$

where $c_{j,\sigma}$ ($c_{j,\sigma}^\dagger$) is the annihilation (creation) operator for an electron at site j and $n_{j,\sigma} = c_{j,\sigma}^\dagger c_{j,\sigma}$. Introducing a local

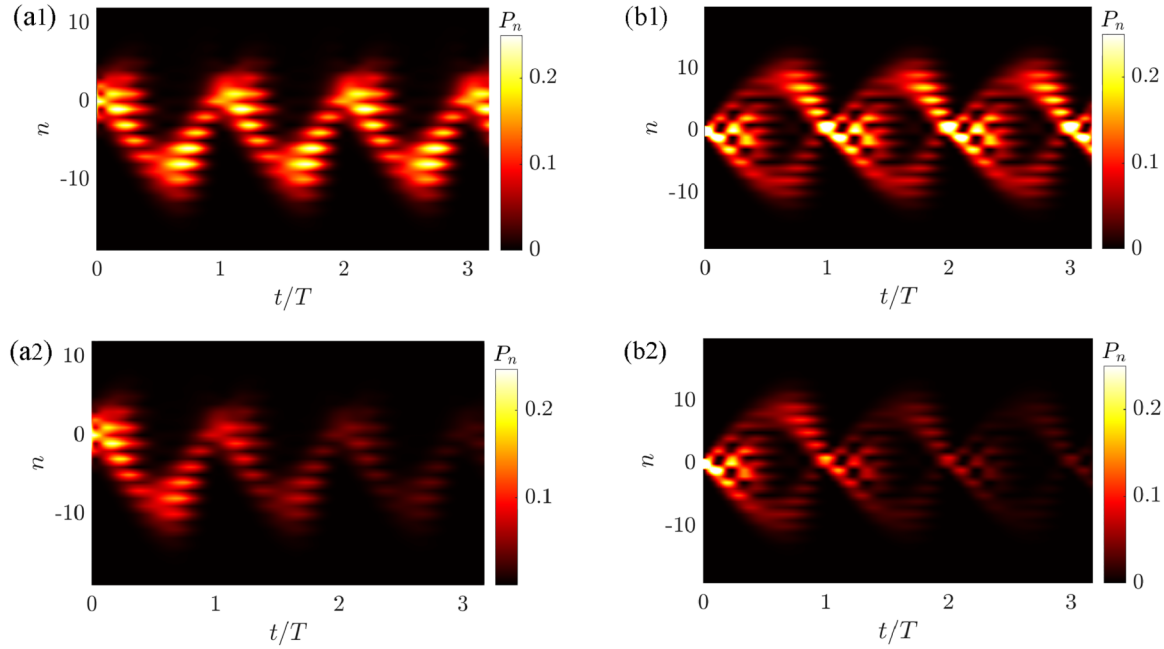

FIG. 3. Plots of $P_n(t)$ defined in Eq. (26), obtained by numerical diagonalization for several different initial states and prefactors with $\omega = 0.2$ and $T = \pi/\omega$. Here, panels (a1) and (a2) correspond to the initial state $e^{-\alpha^2 n^2}(\alpha = 0.3)$ and the prefactors $\lambda = 0.764$ and 0.787, respectively. Panels (b1) and (b2) correspond to the initial state δ_{n0} and the prefactors $\lambda = 0.764$ and 0.787, respectively.

transformation on electron operators

$$\mathcal{P}c_{2j+1,\sigma}\mathcal{P}^{-1} = (-1)^j c_{2j+1,\sigma},$$
$$\mathcal{P}c_{2j,\sigma}\mathcal{P}^{-1} = (-1)^j c_{2j,\sigma}, \tag{28}$$

we have

$$\mathcal{PT}H_{\rm e}(\mathcal{PT})^{-1} = H_{\rm e}, \tag{29}$$

i.e., the system has $\mathcal{PT}$ symmetry.

Now, we focus on the system in a two-electron invariant subspace with opposite spins. Based on the two-electron basis set spanned by $\{|x, y\rangle\}$ where

$$|x, y\rangle = c^\dagger_{x,\uparrow}c^\dagger_{y,\downarrow}|0\rangle, \tag{30}$$

the Hamiltonian can be expressed as a single-particle Hamiltonian on a square lattice [36,37]:

$$\begin{aligned} H_{\rm 2D} = &\sum_{x,y=-\infty}^{\infty}(|2x, y\rangle\langle 2x+1, y| + \text{H.c.}) \\ &+ i\sum_{x,y=-\infty}^{\infty}(|2x-1, y\rangle\langle 2x, y| + \text{H.c.}) \\ &+ \sum_{x,y=-\infty}^{\infty}(|x, 2y+1\rangle\langle x, 2y| + \text{H.c.}) \\ &+ i\sum_{x,y=-\infty}^{\infty}(|x, 2y-1\rangle\langle x, 2y| + \text{H.c.}) \\ &+ \omega\sum_{x,y=-\infty}^{\infty}(x+y)|x, y\rangle\langle x, y|. \end{aligned} \tag{31}$$

Figure 4(a) is a schematic for the structure of $H_{\rm 2D}$. One can check that $H_{\rm 2D}$ has $\mathcal{PT}$ symmetry, i.e.,

$$[\mathcal{PT}, H_{\rm 2D}] = 0, \tag{32}$$

due to the fact

$$\mathcal{P}c^\dagger_{x,\uparrow}c^\dagger_{y,\downarrow}|0\rangle = (-1)^{[x/2]+[y/2]}c^\dagger_{x,\uparrow}c^\dagger_{y,\downarrow}|0\rangle, \tag{33}$$

where $[x]$ represents the greatest integer less than or equal to x.

(ii) For the spinless fermion system, the Hamiltonian reads

$$\begin{aligned} H_{\rm f} = &\sum_j (f^\dagger_{2j}f_{2j+1} + \text{H.c.}) + i\sum_j (f^\dagger_{2j-1}f_{2j} + \text{H.c.}) \\ &+\omega\sum_j jn_j, \end{aligned} \tag{34}$$

where f_j ($f^\dagger_j$) is the annihilation (creation) operator for a fermion at site j and $n_j = f^\dagger_j f_j$. The two-fermion basis set spanned by $\{|x, y\rangle\}$ is defined as

$$|x, y\rangle = f^\dagger_x f^\dagger_y|0\rangle \ (x > y), \tag{35}$$

the Hamiltonian can be expressed as a single-particle Hamiltonian on a square lattice:

$$\begin{aligned} H^+_{\rm 2D} = &\sum_{y=-\infty}^{\infty}\sum_{x=[y/2]+1}^{\infty}(|2x, y\rangle\langle 2x+1, y| + \text{H.c.}) \\ &+ i\sum_{y=-\infty}^{\infty}\sum_{x=[(y+1)/2]+1}^{\infty}(|2x-1, y\rangle\langle 2x, y| + \text{H.c.}) \\ &+ \sum_{x=-\infty}^{\infty}\sum_{y=-\infty}^{[x/2]-1}(|x, 2y\rangle\langle x, 2y+1| + \text{H.c.}) \end{aligned}$$

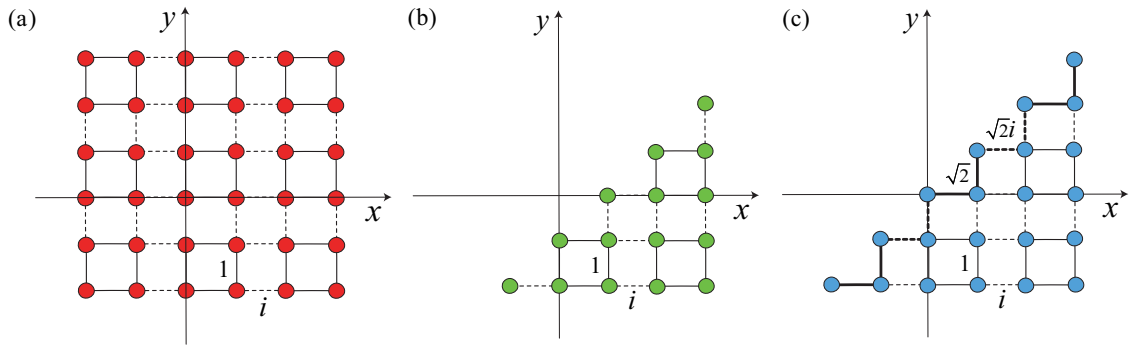

FIG. 4. Schematic illustrations of the Hamiltonians in Eqs. (31), (36), and (39), which are tight-binding models on square lattices with on-site potential $\omega(x+y)$. Panels (a), (b), and (c) can be used to simulate the two-electron, two-spinless-fermions, and two-boson Hamiltonian systems shown in Eqs. (27), (34), and (37), respectively. It can be observed that panel (a) has symmetry along the diagonal direction, while panels (b) and (c) can be obtained by the antisymmetric and symmetric transformations from panel (a), respectively.

$$+i\sum_{x=-\infty}^{\infty}\sum_{y=-\infty}^{[(x-1)/2]}(|x,2y-1\rangle\langle x,2y|+\text{ H.c.})$$
$$+\omega\sum_{x>y}(x+y)|x,y\rangle\langle x,y|. \tag{36}$$

Figure 4(b) is a schematics for the structure of H_{2D}^{+} .

(iii) For the boson system, the Hamiltonian reads

$$H_{\rm b}=\sum_j(b_{2j}^\dagger b_{2j+1}+\text{H.c.})+i\sum_j(b_{2j-1}^\dagger b_{2j}+\text{H.c.})$$
$$+\omega\sum_j jn_j, \tag{37}$$

where b_j ($b_j^\dagger$) is the annihilation (creation) operator for a boson at site j and $n_j=b_j^\dagger b_j$. The two-boson basis set spanned by $\{|x,y\rangle\}$ is defined as

$$|x,y\rangle=b_x^\dagger b_y^\dagger|0\rangle\ (x>y),$$
$$|x,y\rangle=\frac{1}{\sqrt{2}}(b_x^\dagger)^2|0\rangle\ (x=y), \tag{38}$$

and the Hamiltonian can be expressed as a single-particle Hamiltonian on a square lattice:

$$H_{2D}^{-}=H_{2D}^{+}+\sqrt{2}\sum_{y=-\infty}^{\infty}(|2y,2y\rangle\langle 2y+1,2y|+\text{ H.c.})$$
$$+\sqrt{2}\sum_{x=-\infty}^{\infty}(|2x+1,2x\rangle\langle 2x+1,2x-1|+\text{ H.c.})$$
$$+\sqrt{2}i\sum_{y=-\infty}^{\infty}(|2y,2y+1\rangle\langle 2y+1,2y+1|+\text{ H.c.})$$
$$+\sqrt{2}i\sum_{x=-\infty}^{\infty}(|2x,2x\rangle\langle 2x,2x-1|+\text{ H.c.}). \tag{39}$$

Figure 4(c) is a schematics for the structure of H_{2D}^{-} .

One can check that the lattice of H_{2D} has reflection symmetry about the axis $x=y$. Then H_{2D} can be decomposed into two independent sublattices, symmetric and antisymmetric. Notably, systems H_{2D}^{+} and H_{2D}^{-} are just the two corresponding sublattices. The underlying mechanism is the following relation. The singlet two-electron states

$$\frac{1}{\sqrt{2}}(c_{x,\uparrow}^\dagger c_{y,\downarrow}^\dagger-c_{x,\downarrow}^\dagger c_{y,\uparrow}^\dagger)|0\rangle,\quad x\neq y,$$
$$c_{x,\uparrow}^\dagger c_{x,\downarrow}^\dagger|0\rangle,\quad x=y, \tag{40}$$

for $H_{\rm e}$ are equivalent to the two-boson states

$$|x,y\rangle=\begin{cases}b_x^\dagger b_y^\dagger|0\rangle, & x\neq y,\\ \frac{1}{\sqrt{2}}(b_x^\dagger)^2|0\rangle, & x=y,\end{cases} \tag{41}$$

for $H_{\rm b}$. In parallel, the triplet two-electron states

$$|x,y\rangle=\frac{1}{\sqrt{2}}(c_{x,\uparrow}^\dagger c_{y,\downarrow}^\dagger+c_{x,\downarrow}^\dagger c_{y,\uparrow}^\dagger)|0\rangle, \tag{42}$$

for $H_{\rm e}$, are equivalent to the two-spinless-fermion states

$$|x,y\rangle=c_x^\dagger c_y^\dagger|0\rangle, \tag{43}$$

for $H_{\rm f}$. In this sense, the physical properties of both two-boson and two-spinless-fermion systems can be derived from those of the H_{2D} system.

In experiments, single-particle hopping dynamics can be simulated by discretized spatial light transport in an engineered 2D square lattice of evanescently coupled optical waveguides [38]. A 2D lattice can be fabricated by coupled waveguides, by which the temporal evolution of the single-particle probability distribution in the 2D lattice can be visualized by the spatial propagation of the light intensity. According to the non-Hermitian quantum theory, an eigenstate with real energy can be written in the form of $\mathcal{PT}$ symmetry.

We compute the temporal evolution for 2D initial states in the product form

$$|\Phi(0)\rangle=|\varphi_x\rangle|\varphi_y\rangle, \tag{44}$$

where $|\varphi_x\rangle$ and $|\varphi_y\rangle$ are two normalized states for one dimension,

$$|\varphi_x\rangle=\sum_x\mu(x)|x\rangle, \tag{45}$$

$$|\varphi_y\rangle=\mathcal{T}g\sum_y\mu(y)|y\rangle=\sum_y(-1)^{[y/2]}\mu^*(y)|y\rangle. \tag{46}$$

Here, the coefficients $\mu(x)$ can be extracted from the time evolution for the 1D system with initial states $|\phi(0)\rangle$ based

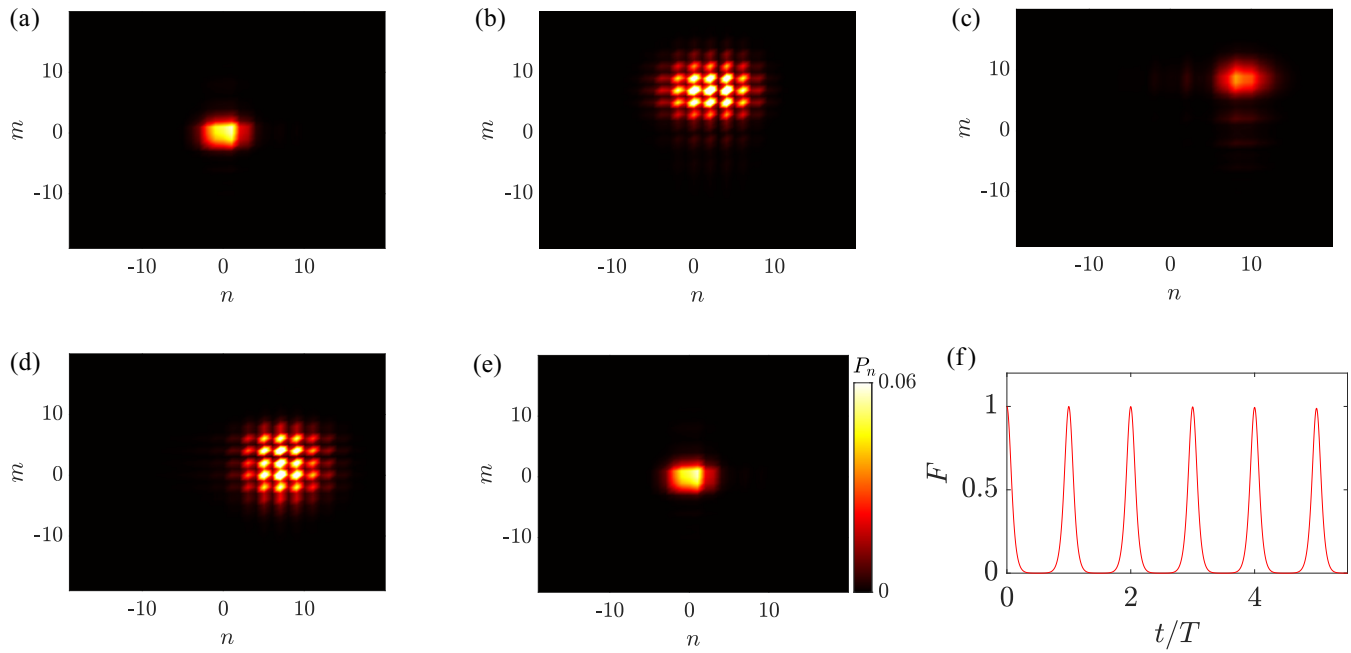

FIG. 5. Plots of $P(x, y, t)$ for several instants defined in Eq. (47) and $F(t)$ defined in Eq. (48), obtained by numerical diagonalization for the initial state $(-1)^{[y/2]}\mu(x)\mu^*(y)$, where $\mu(x)$ is obtained from the long time evolved in Fig. 3(a1). The system parameter $\omega = 0.2$. Here, panels (a)–(e) correspond to the cases with $t = 0, T/4, T/2, 3T/4$, and T, respectively, and panel (f) is the plot of fidelity, indicating a Bloch oscillation.

on the mechanism in Eq. (24). We still employ two types of states, the Gaussian wave-packet state and the site state at the j_0th site.

We calculate the Dirac probability distribution in real space as

$$P(x, y, t) = |\langle x, y|e^{-iH_{2D}t}|\Phi(0)\rangle|^2, \tag{47}$$

and we calculate the fidelity as

$$F(t) = \frac{|\langle\Phi(0)|e^{-iH_{2D}t}|\Phi(0)\rangle|^2}{|e^{-iH_{2D}t}|\Phi(0)\rangle|^2||\Phi(0)\rangle|^2}, \tag{48}$$

for time evolution. We plot $P(x, y, t)$ and $F(t)$ in Figs. 5 and 6 for several typical parameter values. These numerical results agree with our above analysis that the dynamics are periodic for proper initial states. Therefore, we conclude that our result

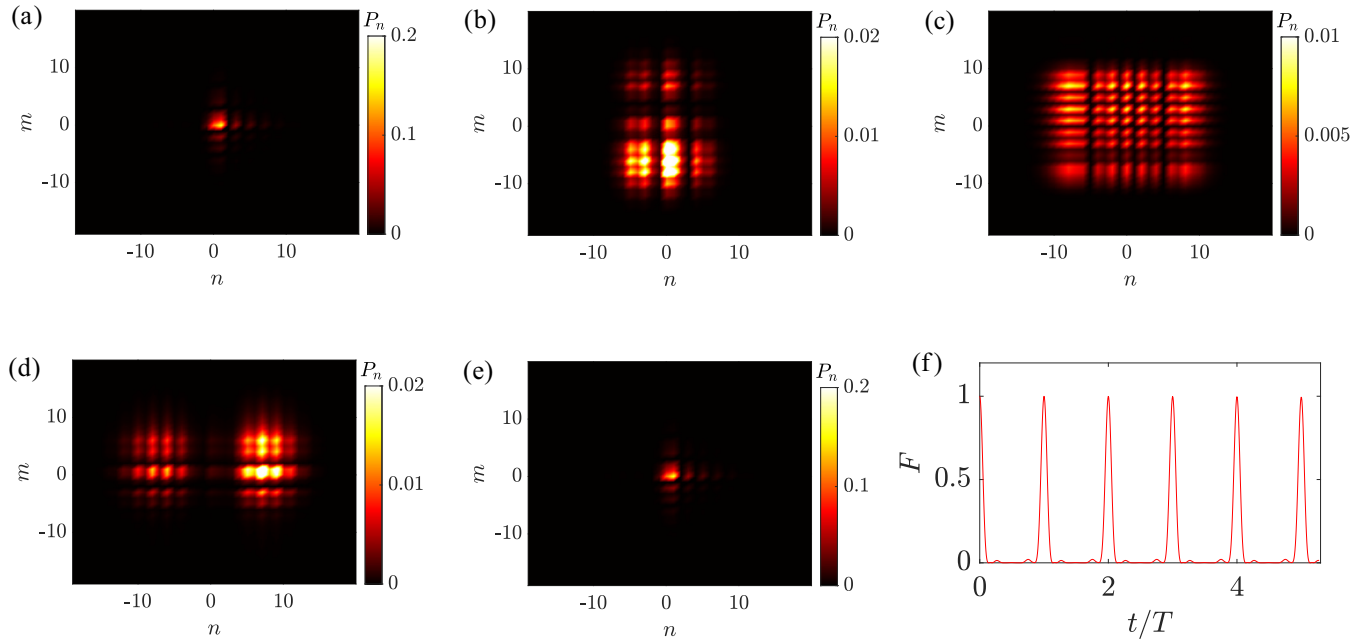

FIG. 6. The same plots as in Fig. 5. Here $\mu(x)$ is obtained from the result in Fig. 3(b1).

for the extended Wannier-Stark ladder in a 1D system can also be applied to a 2D system.

VI. SUMMARY

In summary, our research has investigated the impact of a linear potential on arbitrary periodic systems within the tight-binding model framework, irrespective of the Hermiticity of the system. We have extended the concept of the Wannier-Stark ladder to the complex domain, enabling the analytical prediction of the dynamics for numerous non-Hermitian systems with a constant particle number. We propose two types of dimerized non-Hermitian systems to substantiate our findings. Both analytical analysis and numerical simulations indicate that these dimerized non-Hermitian systems support single-particle Bloch oscillations characterized by a damping (or growing) rate, as well as standard two-particle Bloch oscillations under specific conditions. Furthermore, we demonstrate that the concept of the extended Wannier-Stark ladder, initially developed for 1D systems, is also applicable to 2D systems. We introduce a scheme to illustrate these results through particle-pair dynamics within a single-particle 2D $\mathcal{PT}$-symmetric square lattice. These findings lay the groundwork for exploring a diverse range of periodic systems subjected to a linear potential. The ability to predict the dynamics of such systems analytically is a valuable advancement in the field of condensed-matter physics and quantum mechanics.

ACKNOWLEDGMENTS

This work was supported by the National Natural Science Foundation of China (under Grant No. 12374461).

[1] F. Bloch, Über die quantenmechanik der elektronen in kristallgittern, Z. Phys. **52**, 555 (1929).
[2] G. H. Wannier, *Elements of Solid State Theory* (Cambridge University Press, Cambridge, England, 1959).
[3] G. H. Wannier, Wave functions and effective Hamiltonian for Bloch electrons in an electric field, Phys. Rev. **117**, 432 (1960).
[4] M. Glück, A. R. Kolovsky, and H. J. Korsch, Wannier–Stark resonances in optical and semiconductor superlattices, Phys. Rep. **366**, 103 (2002).
[5] C. Waschke, H. G. Roskos, R. Schwedler, K. Leo, H. Kurz, and K. Köhler, Coherent submillimeter-wave emission from Bloch oscillations in a semiconductor superlattice, Phys. Rev. Lett. **70**, 3319 (1993).
[6] M. Ben Dahan, E. Peik, J. Reichel, Y. Castin, and C. Salomon, Bloch oscillations of atoms in an optical potential, Phys. Rev. Lett. **76**, 4508 (1996).
[7] S. R. Wilkinson, C. F. Bharucha, K. W. Madison, Q. Niu, and M. G. Raizen, Observation of atomic Wannier-Stark ladders in an accelerating optical potential, Phys. Rev. Lett. **76**, 4512 (1996).
[8] B. P. Anderson and M. A. Kasevich, Macroscopic quantum interference from atomic tunnel arrays, Science **282**, 1686 (1998).
[9] O. Morsch, J. H. Müller, M. Cristiani, D. Ciampini, and E. Arimondo, Bloch oscillations and mean-field effects of Bose-Einstein condensates in 1D optical lattices, Phys. Rev. Lett. **87**, 140402 (2001).
[10] R. Morandotti, U. Peschel, J. S. Aitchison, H. S. Eisenberg, and Y. Silberberg, Experimental observation of linear and nonlinear optical Bloch oscillations, Phys. Rev. Lett. **83**, 4756 (1999).
[11] H. Sanchis-Alepuz, Y. A. Kosevich, and J. Sánchez-Dehesa, Acoustic analogue of electronic Bloch oscillations and resonant Zener tunneling in ultrasonic superlattices, Phys. Rev. Lett. **98**, 134301 (2007).
[12] F. Meinert, M. Knap, E. Kirilov, K. Jag-Lauber, M. B. Zvonarev, E. Demler, and H.-C. Nägerl, Bloch oscillations in the absence of a lattice, Science **356**, 945 (2017).
[13] W. Zhang, H. Yuan, H. Wang, F. Di, N. Sun, X. Zheng, H. Sun, and X. Zhang, Observation of Bloch oscillations dominated by effective anyonic particle statistics, Nat. Commun. **13**, 2392 (2022).
[14] U. B. Hansen, O. F. Syljuåsen, J. Jensen, T. K. Schäffer, C. R. Andersen, M. Boehm, J. A. Rodriguez-Rivera, N. B. Christensen, and K. Lefmann, Magnetic Bloch oscillations and domain wall dynamics in a near-Ising ferromagnetic chain, Nat. Commun. **13**, 2547 (2022).
[15] S. Longhi, Bloch oscillations in complex crystals with $\mathcal{PT}$ symmetry, Phys. Rev. Lett. **103**, 123601 (2009).
[16] S. Longhi, Exceptional points and Bloch oscillations in non-Hermitian lattices with unidirectional hopping, Europhys. Lett. **106**, 34001 (2014).
[17] S. Longhi, Bloch oscillations in non-Hermitian lattices with trajectories in the complex plane, Phys. Rev. A **92**, 042116 (2015).
[18] E. M. Graefe, H. J. Korsch, and A. Rush, Quasiclassical analysis of Bloch oscillations in non-Hermitian tight-binding lattices, New J. Phys. **18**, 075009 (2016).
[19] S. Longhi, Non-Hermitian bidirectional robust transport, Phys. Rev. B **95**, 014201 (2017).
[20] T. E. Lee and C.-K. Chan, Heralded magnetism in non-Hermitian atomic systems, Phys. Rev. X **4**, 041001 (2014).
[21] C. M. Bender and S. Boettcher, Real spectra in non-Hermitian Hamiltonians having $\mathcal{PT}$ symmetry, Phys. Rev. Lett. **80**, 5243 (1998).
[22] A. Mostafazadeh, Exact PT-symmetry is equivalent to Hermiticity, J. Phys. A: Math. Gen. **36**, 7081 (2003).
[23] A. Mostafazadeh and A. Batal, Physical aspects of pseudo-Hermitian and PT-symmetric quantum mechanics, J. Phys. A: Math. Gen. **37**, 11645 (2004).
[24] H. F. Jones, On pseudo-Hermitian Hamiltonians and their Hermitian counterparts, J. Phys. A: Math. Gen. **38**, 1741 (2005).
[25] C. M. Bender, S. Boettcher, and P. N. Meisinger, $\mathcal{PT}$-symmetric quantum mechanics, J. Math. Phys. **40**, 2201 (1999).
[26] P. Dorey, C. Dunning, and R. Tateo, Spectral equivalences, Bethe ansatz equations, and reality properties in $\mathcal{PT}$-symmetric quantum mechanics, J. Phys. A: Math. Gen. **34**, 5679 (2001).
[27] C. M. Bender, D. C. Brody, and H. F. Jones, Complex extension of quantum mechanics, Phys. Rev. Lett. **89**, 270401 (2002).

[28] C. M. Bender, Making sense of non-Hermitian Hamiltonians, Rep. Prog. Phys. **70**, 947 (2007).
[29] Y. Ashida, Z. Gong, and M. Ueda, Non-Hermitian physics, Adv. Phys. **69**, 249 (2020).
[30] L. Jin and Z. Song, Physics counterpart of the $\mathcal{PT}$ non-Hermitian tight-binding chain, Phys. Rev. A **81**, 032109 (2010).
[31] X. Z. Zhang, L. Jin, and Z. Song, Perfect state transfer in $\mathcal{PT}$-symmetric non-Hermitian networks, Phys. Rev. A **85**, 012106 (2012).
[32] H. P. Zhang, K. L. Zhang, and Z. Song, Dynamics of non-Hermitian floquet Wannier-Stark system, arXiv:2401.13286.
[33] K. L. Zhang and Z. Song, Magnetic Bloch oscillations in a non-Hermitian quantum Ising chain, Phys. Rev. B **109**, 104312 (2024).
[34] D. N. Maksimov, E. N. Bulgakov, and A. R. Kolovsky, Wannier-Stark states in double-periodic lattices. I. One-dimensional lattices, Phys. Rev. A **91**, 053631 (2015).
[35] D. N. Maksimov, E. N. Bulgakov, and A. R. Kolovsky, Wannier-Stark states in double-periodic lattices. II. Two-dimensional lattices, Phys. Rev. A **91**, 053632 (2015).
[36] G. Corrielli, A. Crespi, G. Della Valle, S. Longhi, and R. Osellame, Fractional Bloch oscillations in photonic lattices, Nat. Commun. **4**, 1555 (2013).
[37] S. Longhi, Photonic Bloch oscillations of correlated particles, Opt. Lett. **36**, 3248 (2011).
[38] D. N. Christodoulides, F. Lederer, and Y. Silberberg, Discretizing light behaviour in linear and nonlinear waveguide lattices, Nature (London) **424**, 817 (2003).